Published in final edited form as:

Nat Commun. ; 6: 6295. doi:10.1038/ncomms7295.

Self-Assembled Hydrogels Utilising Polymer-Nanoparticle Interactions

Eric A. Appel[1,2], **Mark W. Tibbitt**[1,2], **Matthew J. Webber**[1], **Bradley A. Mattix**[1], **Omid Veiseh**[1], and **Robert Langer**[1]

[1]David H. Koch Institute for Integrative Cancer Research, Department of Chemical Engineering, Massachusetts Institute of Technology, Cambridge, MA 02139

Abstract

Mouldable hydrogels that flow upon applied stress and rapidly self-heal are increasingly utilised as they afford minimally invasive delivery and conformal application. Here we report a new paradigm for the fabrication of self-assembled hydrogels with shear-thinning and self-healing properties employing rationally engineered polymer-nanoparticle interactions. Biopolymer derivatives are linked together by selective adsorption to nanoparticles. The transient and reversible interactions between biopolymers and nanoparticles enable flow under applied shear stress, followed by rapid self-healing when the stress is relaxed. We develop a physical description of polymer-nanoparticle gel formation that is utilised to design biocompatible gels for minimally-invasive drug delivery. Owing to the hierarchical structure of the gel, both hydrophilic and hydrophobic drugs can be entrapped and delivered with differential release profiles, both *in vitro* and *in vivo*. The work introduces a facile and generalizable class of mouldable hydrogels amenable to a range of biomedical and industrial applications.

Introduction

Hydrogels comprise an important class of material well-suited for a range of applications on account of their high water content and highly tunable mechanical properties.[1–4] Many hydrogel systems utilise covalent crosslinking approaches,[5] including radical processes initiated by light,[6,7] temperature,[8] and pH.[9] These covalently crosslinked hydrogels form robust, tough and elastic materials; however, they can be limited by the irreversibility of their crosslinks. Mouldable hydrogels that can be formed and processed prior to use and

Correspondence to: Robert Langer.

[2]These authors contributed equally to this work.

Author contributions

E.A.A., M.W.T., and R.L. conceived the ideas. E.A.A., M.W.T., M.J.W., and R.L. designed the experiments. E.A.A., M.W.T., M.J.W., B.A.M., and O.V. conducted the experiments and analysed the data. E.A.A., M.W.T., M.J.W., and R.L. interpreted the data and wrote the manuscript.

Supplementary information accompanies this paper at www.nature.com.

Animal Protocols

All animal procedures were performed according to MIT Animal Care and Use Committee approved protocols.

Competing Financial Interests

The authors declare no competing financial interests.

subsequently applied in a conformal manner provide attractive alternatives to covalent hydrogels for many applications, including local drug delivery applications in the body, cell carriers for tissue engineering, bone fillers, or hydraulic fracturing fluids. To serve these applications, mouldable hydrogels must exhibit viscous flow under shear stress (shear-thinning) and rapid recovery when the applied stress is relaxed (self-healing). Additionally, it is extremely beneficial if the high shear viscosity is low ($\eta \leq 1$ Pa s @ $\dot{\gamma} \sim 100$ s^{-1}) for facile application through high gauge needles. These properties enable minimally invasive implantation *in vivo* though direct injection or catheter-based delivery, contributing to a rapid gain in interest in their application for controlled drug delivery.[10]

Self-assembly *via* non-covalent crosslinking provides a route to fabricate mouldable and injectable hydrogels with shear-thinning and self-healing properties arising from strong, yet transient and reversible crosslinks.[2,10] Several systems have been reported utilising natural host-guest or receptor-ligand pairs, such as (strep)avidin with biotin,[11,12] leucine zipper[13,14] and 'dock-and-lock'[15,16] protein structures prepared with genetic engineering techniques, or with synthetic macrocyclic host molecules, such as cyclodextrins[17,18] or cucurbit[*n*]urils.[19–23] In each of these examples, self-assembly of functional materials *via* non-covalent, intermolecular interactions with dynamic and reversible macroscopic behaviour was exploited. However, the shear-thinning and self-healing hydrogels presented to date are limited by poor mechanics and slow self-healing or require challenging, costly and poorly scalable synthesis of macromolecular components through protein engineering or complex, multi-step functionalisation chemistries.

Crucial requirements to the biomedical translation of mouldable and injectable hydrogels are facile and mild formation, modular modification and finely tunable control over mechanical properties, as well as rapid self-healing upon injection. Within the field of self-assembly, polymer-nanoparticle interactions have arisen as a simple route to assemble tunable and self-healing polymeric materials without the need for complex synthetic approaches or specialised small-molecule binding partners.[24,25] For example, complementary affinity between polymers (molecular binders) and the surface of hard nanoparticles (clay nanosheets/silicates) has been utilised to fabricate high-water-content and mouldable hydrogels.[24,26–28] More recently, nanoparticle adsorption to polymer gels has been exploited to achieve strong, rapid adhesion between disparate gels.[25] Moreover, a similar phenomenon has been exploited to enhance the bulk mechanical properties of polysaccharide-based physically crosslinked hydrogels by incorporating drug-loaded poly(lactic-*co*-glycolic acid) (PLGA) microspheres into the hydrogel formulation.[29,30]

Inspired by these elegant approaches, we synthesise shear-thinning and self-healing hydrogels in a mild, modular and scalable fashion based solely on interactions between cellulose derivatives and nanoparticles for biomedical applications. Herein, we report the preparation and application of hydrogels driven by non-covalent interactions between hydroxypropylmethylcellulose derivatives (HPMC-*x*) and core-shell nanoparticles (NPs) (Fig. 1). Transient and reversible interactions between the NPs and HPMC chains govern polymer-nanoparticle (PNP) hydrogel self-assembly, allowing for flow under applied stress and complete recovery of their structural properties when the stress is relaxed. PNP hydrogels are formulated with PEG-*b*-PLA NPs to enable dual loading of a hydrophobic

molecule into the PEG-*b*-PLA NPs and a second, hydrophilic molecule into the aqueous bulk of the gel. PEG-*b*-PLA PNP hydrogels are biocompatible and afford differential release of multiple compounds *in vivo* following subcutaneous implantation.

Results

Polymer-nanoparticle hydrogels

Initially, polymer-nanoparticle (PNP) hydrogels were formed by mixing aqueous solutions of hydroxypropylmethylcellulose (HPMC; M_n ~ 700 kDa) and commercially available carboxy-functionalised polystyrene nanoparticles (PSNPs; D_H ~ 50 nm; 1 wt% HPMC : 10 wt% PSNPs) under ambient conditions (Fig. 2a). These gels formed rapidly upon mixing, exhibiting a shear storage modulus of G' = 140 Pa. For these studies, the storage modulus (G') was used as a measure of hydrogel *strength*, and the tanδ, which is the ratio of the loss modulus (G'') over the storage modulus (tan$\delta = G''/G'$), was used as a measure of hydrogel *elasticity*. HPMC was chosen as the primary polymer for preparation of PNP hydrogels on account of its high solubility, molecular weight, functionality, and biocompatibility.[31] PSNPs enable a systematic investigation of the effect of NP number and NP diameter (D_H ~ 50 to 500 nm), with uniform surface properties, on PNP gel formation. Hydrogel formation is exclusive to the presence of both PSNPs and HPMC as PSNPs (10 wt%) and HPMC (1 wt %) solutions alone are each low viscosity liquids. Cryogenic transmission electron microscopy (TEM) indicates that the nanoparticles remain homogeneously dispersed in the gel state, suggesting that gel formation is driven by polymer-nanoparticle interactions and not agglomeration (Fig. S8). Moreover, HPMC combined with commercially available silica NPs (Ludox TM-50; d ~ 22 nm; 1 wt% HPMC : 10 wt% NPs) failed to form a gel. These data indicated that selective adsorption of HPMC chains to PSNPs enables cross-linking and gel formation.

Efficient crosslinking necessitates strong affinity between the nanoparticles and the polymer chains, *i.e.* the free energy gain (ε) resulting from adsorption of a polymer chain to the surface of a nanoparticle should be greater than or comparable to the thermal energy (k_BT). Additionally, the average number of interactions per polymer chain (m)$^-$and particle (w)$^-$ must be greater than 2 to achieve percolation of the network. Moreover, in order to favour polymer bridging of multiple nanoparticles (as opposed to polymer wrapping around individual particles), the nanoparticle diameter should be comparable to, or less than, the persistence length (l_P) of the polymer strands. When these criteria are met, nanoparticles act as crosslinkers between the polymer chains, whilst the polymer chains bridge many different particles, enabling hydrogel formation. The modulus (G) of the PNP hydrogels can be related to the number of polymer-nanoparticle interactions per unit volume (n) and the energy associated with each interaction (αk_BT) using theoretical tools analogous to those developed for covalent hydrogels: $G \approx n \cdot \alpha k_BT$.[32]

Based on this physical picture of PNP hydrogels, we hypothesised that hydrophobic modification of HPMC (yielding HPMC-x) could be exploited to increase the energy associated with each PNP interaction (αk_BT), thereby increasing the modulus of the gel given the same number of interactions per unit volume. Modification should facilitate favorable interactions between the hydrophobic moiety on the HPMC chain and the

hydrophobic core of the PSNPs, thereby enhancing the adsorption energy of the HPMC to the NPs. HPMC was readily functionalised using commercially available isocyanates (including hexyl, adamantyl, and dodecyl isocyanate; Supplementary Table 1) in a one-step reaction performed at ambient temperature using dibutyltin dilaurate (TDL) as a catalyst.[33] PNP gels were then formulated with HPMC-*x*, where *x* refers to hexyl (C_6), adamantyl (Ad), or dodecyl (C_{12}) functionality, and PSNPs (D_H ~ 50 nm; 1 wt% HPMC-*x* : 10 wt% PSNPs). PNP gels formed with either HPMC-C_6 or HPMC-Ad possessed similar properties to unmodified HPMC gels. However, PNP gels formed with HPMC-C_{12} were roughly three times stronger (G' = 400 Pa), indicating an increased interaction energy between the C_{12} moieties and the PSNPs (Fig. 2a). These observations are particularly appealing as the rheology of the HPMC-C_{12} polymer at 1 wt% is characteristic of a low viscosity fluid, despite conjugation of hydrophobic moieties (Supplementary Figure 3) and the polymer's ability to form hydrogels are higher concentrations.[34]

Additionally, we investigated the effect of nanoparticle number and size on PNP gel formation. We hypothesised that gel modulus would scale directly with the number of NPs and that particle sizes below a critical diameter, expected to be comparable to the persistence length of the polymer (l_P ~ 90 nm for HPMC) in order to facilitate bridging between particles, would favour gel formation. The number of nanoparticles in the PNP gels was modulated by formulating PNP solutions with decreasing fractions of PSNPs (1 wt% HPMC-C_{12} : 10, 5, or 1 wt% PSNPs with D_H ~ 50 nm). The shear storage modulus (G') decreased, as predicted, with fewer NPs, and consequently, decreasing number of polymer-nanoparticle interactions per unit volume (n) (Fig. 2b).

Next, we screened PNP gel formation with PSNPs of various sizes (D_H ~ 50, 75, 100, 200, and 500 nm; 1 wt% HPMC-C_{12} : 10 wt% PSNPs). We observed that robust gels formed with particle diameters equal to or less than 100 nm, whereas larger particles failed to produce gels (Fig. 2c). These observations support our hypothesis that $D_H \leq l_P$ favour gel formation; yet, this set of experiments was confounded by the fact that as particle diameter increases for a given loading, the particle number decreases. To further elucidate the effect of particle size on PNP gel formation, we formulated a PNP gel composed of HPMC-C_{12} (1 wt%) and both 50 nm PSNPs (5 wt%) and 500 nm PSNPs (1, 3 and 5 wt%). As large particles are titrated into the PNP gels, a monotonic decrease in material properties was observed (Fig. 2d), highlighting the importance of the critical particle size in PNP gel formulations.

Strain dependent oscillatory rheology (Fig. 2e) of the HPMC-C_{12} PNP gels (1 wt% HPMC-C_{12} : 10 wt% 50 nm PSNPs) displayed an extremely broad linear viscoelastic region in addition to network failure at high strains, indicating a wide processing regime and shear-thinning behaviour. The frequency dependence of the storage and loss oscillatory shear moduli (G' and G'', respectively) confirmed hydrogel-like behaviour as G' is dominant across the whole range of frequencies observed (0.1 – 100 rad/s; Fig. 2f). Step-strain measurements were then performed to investigate the recovery of material properties following network rupture at high strains (a critical parameter for injectability). A high magnitude strain (ε = 500 %) was applied to break the hydrogel structure, followed by a low magnitude strain (ε = 0.5 %) to monitor the rate and extent of recovery of bulk properties

(Fig. 3a). These materials exhibit exceptionally fast and complete recovery of properties in a matter of a few seconds after stress-induced flow. Moreover, the rate and extent of recovery is unchanged over several cycles of breaking and reforming, highlighting the reversible and robust nature of the non-covalently crosslinked hydrogel structure (Fig. 3b).

The rheology of PNP gels supports the physical picture of gel assembly. Polymer adsorption to core-shell nanoparticles drives PNP formation. Gel properties are influenced by the energetic favourability of adsorption (enhanced by hydrophobicity of the HPMC), number of polymer-nanoparticle interactions, as well as the diameter of the nanoparticles. Moreover, the transient and reversible nature of polymer adsorption to the nanoparticles imparts the PNP gels with shear-thinning and rapid self-healing properties. When the hydrogel is strained, chains adsorbed to the particles are under tension and detach from the particle surface in order to relax this tension. In this manner, polymer–nanoparticle interactions retard failure and ensure strong crosslinking as the energy dissipated during the stress-induced desorption is much greater than $\varepsilon \sim k_B T$. Additionally, these interactions allow the gel to flow with sufficient applied stress (*shear-thinning*) as polymers desorb and slide past one another. Upon relaxation of the applied stress, the gel rapidly re-forms (*self-healing*) as polymers adsorb to particles in a new configuration.

PNP hydrogels from biodegradable nanoparticles

With robust design principles in hand, we sought to develop PNP gels composed of biocompatible and biodegradable nanoparticles. Poly(ethylene glycol)-*block*-poly(lactic acid) (PEG-*b*-PLA) core-shell NPs have been employed as drug delivery vehicles in a range of *in vivo* applications[35,36] and presented a promising candidate for PNP gels as they can be formed with D_H ~ 100 nm in a reproducible and scalable manner. PEG_{5k}-*b*-PLA_{20k} block copolymers were prepared *via* organocatalytic ring opening polymerisation utilising 1,8-diazabicylo-undec-7-ene (DBU) as a catalyst (Fig. 1c).[37] Core-shell NPs ($D_H \approx 100$ nm according to dynamic light scattering) were prepared by nano-precipitation of the amphiphilic diblock copolymer from DMSO (a good solvent for both blocks) into water (a selective solvent for the hydrophilic PEG block).[38] These synthetic protocols are facile, rapid and are easily scaled.

As before, mixing aqueous solutions of HPMC-C_{12} and PEG-*b*-PLA NPs produced a PNP hydrogel (HPMC-C_{12} 1 wt% : PEG-*b*-PLA NPs 10 wt%) with analogous mechanical properties (Fig. 4a and b). The presence of the PEG corona on the NPs dramatically reduced the inherent affinity between the HPMC and the NPs, resulting in a 30-fold increase in shear storage modulus with conjugation of C_{12} moieties (Fig. 4a). Thus, strong adhesion between HPMC-*x* polymers and PEG-*b*-PLA NPs, and consequent hydrogel formation, requires the presence of a sufficiently long hydrophobic tail. Moreover, decreasing the size of the PEG corona on the NPs by employing block copolymers with a shorter PEG chain (PEG_{2k}-*b*-PLA_{16k}) led to enhanced polymer-nanoparticle interactions and stronger materials (Supplementary Figure 6). Furthermore, the dynamic nature of the non-covalent interactions is retained in these materials, affording similar stress-induced flow properties and material recovery as for hydrogels formulated with PSNPs (Fig. 4c and d). The shear-thinning behaviour on these materials was further investigated with steady shear measurements

(Supplementary Figure 7), which indicated a large change in the viscosity ($\Delta\eta \sim 10^3$ Pa s) from low ($\dot{\gamma} \sim 0.1$ s^{-1}) to high ($\dot{\gamma} \sim 100$ s^{-1}) shear rates, a beneficial property for facile injection through high gauge needles.

In vitro controlled drug release

As PNP hydrogels composed of PEG-*b*-PLA NPs contain both hydrophilic and hydrophobic domains, we hypothesised that dual encapsulation and controlled release of therapeutics was possible with these materials (Fig. 5a). Moreover, as the PEG-*b*-PLA NPs constitute a structural component of the gel, we sought to characterise the gel's ability to impart differential release characteristics to multiple cargo. We first encapsulated fluorescein-labeled bovine serum albumin (BSA-FITC), a model protein therapeutic, into the aqueous phase of the hydrogels by dissolving it into the HPMC-C_{12} solution prior to hydrogel formation. The BSA was completely retained within the hydrogels upon formation and the release of the BSA into water (an infinite sink) was monitored using UV-vis spectroscopy. The release profile (Fig. 5b) appeared to be first-order and governed by Fickian diffusion.[39] Modeling of the release data according to the Ritger-Peppas equation[40] confirmed diffusional albumin release (k = 0.031±0.001 %/h; Fig. 5c).

In stark contrast to these observations, a model hydrophobic drug compound, Oil Red, which was encapsulated into the PEG-*b*-PLA NPs during the nanoprecipitation process[38] prior to hydrogel formation, were released from the hydrogels with an entirely different profile (Fig. 5d). This model drug demonstrated a small burst release (<10%), followed by zero-order release (k = 2.0±0.6 ×10^{-4} %/h), attributable to erosion-based release. Indeed, when the release supernatant is observed by DLS, nanoparticles of a similar D_H are observed, indicating that intact particles release from the gel through an erosion-based mechanism (Fig. 5e). Thus, PNPs exploit PEG-*b*-PLA NPs as a structural component of the material as well as a carrier motif allowing for multiple therapeutics to be encapsulated simultaneously and released with differential profiles. Previous studies with similar nanocomposite drug delivery systems, employing drug-loaded poly(lactic-*co*-glycolic acid) (PLGA) nanospheres as mechanical enhancers of physical hydrogel blends, have demonstrated release of both hydrophilic (1 to 4 days) and hydrophobic (up to 30 days) species *in vitro via* similar mechanisms.[30]

In vivo implantation and controlled drug release

Having synthesised injectable hydrogels with unique drug delivery profiles, we sought to characterise the *in vivo* utility of PNP gels (1 wt% HPMC-C_{12} : 10 wt% PEG-*b*-PLA NPs). First, adult C57BL/6 mice were injected subcutaneously with PNP hydrogels and a phosphate buffered saline (PBS) bolus as a control. While the PBS bolus dissipated in less than an hour, the PNP hydrogel, which reformed immediately upon injection, remained intact at 7 days (Supplementary Figure 9) The injected materials were harvested after 3 and 7 days and histological anaylsis (Fig. 6) demonstrated mild infiltration of the material by neutrophils at day 3, which were replaced primarily by macrophages at day 7. The material was beginning to be cleared by macrophages at this time, with no evidence of multi-nucleated giant cells or lymphocytes, no indication of fibrosis, and no signs of inflammation

or damage in the adjacent tissue (additional histological analysis is contained in Supplementary Figures 10 and 11).

Based on the favourable biocompatibilty of the gels, PNP gels were formulated with a model hydrophobic therapeutic (Texas Red® -DHPE; TR) loaded into PEG-*b*-PLA NPs and a model hydrophilic protein therapeutic, Alexa Fluor® 680-conjugated BSA (BSA-AF), loaded into the aqueous bulk of the gel, to investigate their *in vivo* release characteristics. Adult SKH1E (hairless) mice were injected subcutaneously with these dual-"therapeutic"-loaded PNP gels and the release was monitored *via* intravital fluorescence imaging (Fig. 7a). It was not possible to quantitatively investigate the release rate of the model therapeutics from the hydrogel *in vivo* on account of photobleaching of the TR dye and changing PNP hydrogel size on account of its mouldability. Yet, a consistent release pattern was observed in the SKH1E mice (n = 5) wherein the BSA accessed more of the animal than the TR. With a cut-off value of 20% relative intensity, fluorescent analysis revealed that the BSA was present ~ 10 mm from the injection site whereas the TR remained within ~ 4 mm of the injection site. (Fig. 7b–d). Control experiments with BSA-AF alone (bolus injection) and BSA-AF with HPMC-C_{12} (Supplementary Figure 13) indicate that BSA release is governed primarily by interactions between BSA and HPMC-C_{12} and not hydrogel network constraints. Furthermore, control experiments with TR-loaded particles alone (Supplementary Figure 14) highlight that PNP hydrogels enable simultaneous release of both hydrophobic and hydrophilic molecular cargo *in vivo* from a single gel.

Discussion

In summary, we have prepared shear-thinning injectable hydrogels utilising polymer-nanoparticle interactions between hydrophobically-modified cellulose derivatives (HPMC-*x*) and nanoparticles (NPs). Transient and reversible hydrophobic forces between the NPs and HPMC chains govern the self-assembly of hydrogels, enabling them to flow under applied shear stress and facilitating complete recovery of their material properties in a matter of seconds when the stress is relaxed. Moreover, biocompatible hydrogels formulated with PEG-*b*-PLA NPs enable dual loading of a hydrophobic molecule into the PEG-*b*-PLA NPs and a second, hydrophilic molecule into the aqueous bulk of the gel. Owing to the hierarchical structure of the gel, molecular delivery is controlled both by Fickian diffusion and erosion-based release affording differential release of multiple compounds from a single material, *in vitro* and *in vivo*. The biocompatibility of these materials and the differential release of multiple loaded model therapeutics was demonstrated *in vivo*. Overall, this manuscript demonstrates a class of injectable hydrogels for controlled drug delivery applications with facile synthesis and minimally invasive implantation *in vivo*.

Methods

Instrumentation and Materials

^{1}H NMR (400 MHz) spectra were recorded using a Bruker Avance QNP 400. Chemical shifts are recorded in ppm (δ) in H_2O with the internal reference set to δ = 4.80 ppm. ATR FT-IR spectroscopy was performed using a Perkin-Elmer Spectrum 100 series FT-IR spectrometer equipped with a universal ATR sampling accessory. Gel permeation

chromatography (GPC) was carried out in either tetrahydrofuran (THF) on divinylbenzene columns or in H_2O on glucose-modified divinylbenzene columns, both utilizing a Malvern Viscotek™ TDA 305 triple detection system. Samples were filtered over 0.2 μm PTFE (THF) or PVDF (H_2O) filters before injection using a 1.0 mL/min flow rate. Molecular weights and polydispersities were determined by comparing to either PMMA (THF) or dextran (H_2O) standards. Dynamic light scattering (DLS) measurements were performed with a Malvern Instruments Zetasizer Nano-ZS.

Rheological characterisation was performed using a TA Instruments AR-G2 stress controlled rheometer fitted with a Peltier stage set to 37 °C. Dynamic oscillatory strain amplitude sweep measurements were conducted at a frequency of 10 rad/s (unless otherwise noted). Dynamic oscillatory frequency sweep measurements were conducted at a 2% strain amplitude (unless otherwise noted). All measurements were performed using a 20 mm 4° cone geometry and analyzed using TA Instruments TRIOS software.

Cryogenic scanning electron microscopy (CryoSEM) images of PNP gels where acquired using a Zeiss NVision 40 (Carl Zeiss SMT, Inc.) field emission scanning electron microscope at an acceleration voltage of 2 kV. To prepare samples for imaging approximately 100 μL of gel was transferred to a sample stub and then plunged into a slushy (liquid and solid) nitrogen bath. The samples where next transferred to an EM VCT100 vacuum cryo-transfer system (Leica Microsystems, Inc.) to selectively remove surface water (vitreous ice) by controlled specimen sublimation. The frozen sample were then further fractured with a sharp blade and sputter coated with a thin layer of platinum and palladium metals prior to imaging.

Cryogenic transmission electron microscopy (CryoTEM) images where acquired using a JEOL 2100 FEG microscope (Jeol Inc. Peabody, MA) equipped with an Gatan 2kx2k UltraScan CCD camera at an acceleration of 200 kV and at magnification ranges of 10,000–30,000x. To prepare samples for imaging, approximately 3 μL of nanoparticle suspensions was transferred to a lacey copper grid (coated with continuous carbon). Next, using a Gatan Cryo Plunge III the grids where blotted with great care to remove any excess liquid without causing damage to the carbon layer. The prepared grids where then mounted on a Gatan 626 cryo-holder equipped in the TEM column. The specimen and holder tips were next cooled down using liquid nitrogen, and subsequently transferred to the CryoTEM for imaging.

Monomethoxy-poly(ethylene glycol) (PEG; 5 kDa) was purchased from Aldrich and was purified by azeotropic distillation with toluene. Lactide (LA) was purchased from Aldrich and dried in a desiccator over P_2O_5 prior to use. Carboxy-functional poly(styrene) nanoparticles (PSNPs) were purchased from Phosphorex and used as received. All other materials were purchased from Aldrich and used as received.

General synthesis of HPMC-*x* polymers

HPMC (1.0 g) was dissolved in *N*-methylpyrrolidone (NMP; 45 mL) by stirring at 80 °C for 1 h. Once the solution had cooled to room temperature, a solution of 1-hexylisocyanate, 1-adamantylisocyanate, or 1-dodecylisocyanate (0.5 mmol) and triethylamine (2 drops) was dissolved in NMP (5 mL) and added to the reaction mixture, which was then stirred at room

temperature for 16 h. This solution was this precipitated from acetone and the polymer was recovered by filtration, dried under vacuum at room temperature for 24 h and weighed, yielding the functionalised HPMC as a white amorphous powder (0.96 g, 96%). FT-IR: $\tilde{\nu}$ = 1685, 1601, 1367 cm^{-1}.

PEG-*b*-PLA synthesis

PEG (0.25 g, 4.1 mmol) and 1,8-diazabicycloundec-7-ene (DBU; 10.6 mg, 10 μL, 1.0 mol% relative to LA) was dissolved in DCM (1.0 mL). Lactide (LA; 1.0 g, 6.9 mmol) was dissolved in DCM (3.0 mL) with mild heating. The LA solution was then added rapidly to the PEG/DBU solution and was allowed to stir rapidly for 10 min. The reaction mixture was then quenched by addition of acetone (7.0 mL) and the PEG-*b*-PLA copolymer was recovered by precipitation from cold diethyl ether, collected by filtration, and dried under vacuum to yield a white amorphous polymer (1.15 g, 92%). GPC (THF): M_n (PDI) = 25 kDa (1.09).

PEG-*b*-PLA NP preparation

A solution of PEG-PLA in DMSO (40 mg/mL) was added dropwise to water (10× v/v) under a high stir rate. NPs were purified by ultracentrifugation over a filter (MWCO 30 kDa) followed by resuspension in water to a final concentration of 150 mg/mL. NP size and dispersity were characterised by dynamic light scattering (DLS) with a Malvern Zetasizer Nano-ZS.

PNP gel preparation

PNP gels were prepared by first dissolving HPMC polymers in water (30 mg/mL) with stirring and mild heating. Nanoparticles were either purchased or prepared according to literature procedures[38] and were concentrated to 15 wt% solutions. HPMC polymer solution (150 μL) and NP solution (300 μL) were then added together and mixed well by vortex (some samples were mildly centrifuged to remove bubbles arising from mixing).

PNP gel characterisation

Rheological characterisation was performed using a TA Instruments AR-G2 controlled stress rheometer fitted with a Peltier stage. All measurements were performed using a 40 mm 2° cone geometry and analysed using TA Instruments TA Orchestrator software. CryoSEM images where acquired using a Zeiss NVision 40 (Carl Zeiss SMT, Inc.) field emission scanning electron microscope at an acceleration voltage of 2 kV. CryoTEM images where acquired using a JEOL 2100 FEG microscope (Jeol Inc. Peabody, MA) equipped with an Gatan 2kx2k UltraScan CCD camera at an acceleration of 200 kV and at magnification ranges of 10,000–30,000x.

In vitro release

Two experiments were designed to investigate encapsulation and release of a hydrophobic molecule (Oil Red dye; OR) and a hydrophilic molecule (Bovine Serum Albumin; BSA). For the first experiment, hydrogels were prepared as mentioned above except with FITC-labeled BSA dissolved alongside the HPMC polymer, resulting in a final concentration of

BSA of 1 wt% in the hydrogel. For the second experiment, OR-loaded PEG-PLA NPs were prepared by co-nanoprecipitation of OR with PEG-PLA block copolymer. These NPs were then used to prepare hydrogels as above. Hydrogel of either type (200 μL) was placed into a 1.5 mL centrifuge tube and deionised water (1.3 mL) was added on top of the hydrogel. This setup was placed into an incubator at 37 °C and 1 mL of the aqueous supernatant solution was replaced with fresh deionised water at predetermined time intervals. The collected aqueous solutions were analyzed for solute concentration based on calibration curves prepared using either OR or FITC-Albumin absorbance. All experiments were performed in triplicate.

In vivo biocompatibility studies

All animal procedures were performed according to MIT Animal Care and Use Committee approved protocols. For biocompatibility studies, adult male C57BL/6 mice (8 weeks old) were injected subcutaneously on the back with PNP gels (200 μL; HPMC-C_{12} 1 wt% : PEG-*b*-PLA NPs 10 wt%) using a 26G syringe. At 3 and 7 days following administration, mice were euthanised and the hydrogel and surrounding tissue was harvested (3 mice per time point). Tissue was fixed for 24 hours in formalin and cross-sections of the skin and underlying material (~ 40 μm in thickness), embedded in paraffin, were stained with standard haematoxylin and eosin (H&E) or Mason's trichrome.

In vivo release studies

PNP gels were prepared with BSA-AF (10 μM in the final gel; Life Technologies) loaded into the aqueous phase and Texas Red® -DHPE encapsulated within the PEG-*b*-PLA NPs ([TR] = 10 μM in the final gel). Control hydrogels, containing only one of the fluorescent compounds, were similarly prepared. Adult male SKH1E mice (8 weeks old) were injected subcutaneously on the back with PNP gels (200 μL; HPMC-C_{12} 1 wt% : PEG-*b*-PLA NPs 10 wt%) using a 26G syringe. For *in vivo* imaging, 8-week old male hairless SKH1-E mice were first maintained on an alfalfa-free diet for two weeks prior to administration to limit background fluorescence. Mice were anesthetised using inhaled isoflurane, and 200 μL was injected subcutaneously into the rear right flank of the animal using a 26G syringe. Treatment groups consisted of the hydrogel with the combined fluorophores (n=5), the control hydrogel with TR only (n=2), the control hydrogel with BSA-AF only (n=2), a bolus injection of TR-loaded NPs (n=3), an injection of BSA-AF with HPMC-C_{12} (n=3), and a bolus injection of BSA-AF in PBS (n=1). Imaging was conducted on an IVIS® Spectrum *in vivo* imaging system with a heated stage and an inhaled isoflurane manifold. Fluorescent images were collected at several time-points over the following week, using filter sets of 570/620 (Texas Red) and 675/720 (AF-680) with a 1.5 cm subject height using small binning and an F-stop of 1.

Supplementary Material

Refer to Web version on PubMed Central for supplementary material.

Acknowledgments

E.A.A. is extremely grateful for financial support through a Wellcome Trust-MIT Postdoctoral Fellowship. M.W.T. is extremely grateful for financial support from the Misrock Foundation through a Cancer Nanotechnology Postdoctoral Fellowship. O.V. acknowledges support from CDMRP, Department of Defense, postdoctoral fellowship award (W81XWH-13-1-0215). The work is supported by NIH-R01 DE016516.

References

1. Lutolf MP, Hubbell JA. Synthetic Biomaterials as Instructive Extracellular Microenvironments for Morphogenesis in Tissue Engineering. Nat Biotechnol. 2005; 23:47–55. [PubMed: 15637621]
2. Appel EA, del Barrio J, Loh XJ, Scherman OA. Supramolecular Polymeric Hydrogels. Chem Soc Rev. 2012; 41:6195–6214. [PubMed: 22890548]
3. Hoffman AS. Hydrogels for Biomedical Applications. Adv Drug Delivery Rev. 2002; 54:3–12.
4. Tibbitt MW, Anseth KS. Dynamic Microenvironments: The Fourth Dimension. Sci Trans Med. 2012; 4:160ps24.
5. Pritchard CD, et al. An Injectable Thiol-Acrylate Poly(ethylene glycol) Hydrogel for Sustained Release of Methylprednisolone Sodium Succinate. Biomaterials. 2011; 32:587–597. [PubMed: 20880573]
6. Obara K, et al. Photocrosslinkable Chitosan Hydrogel Containing Fibroblast Growth Factor-2 Stimulates Wound Healing in Healing-Impaired db/db Mice. Biomaterials. 2003; 24:3437–3444. [PubMed: 12809772]
7. Burdick JA, Anseth KS. Photoencapsulation of osteoblasts in injectable RGD-modified PEG hydrogels for bone tissue engineering. Biomaterials. 2002; 23:4315–4323. [PubMed: 12219821]
8. Wu DQ, et al. Fabrication of Supramolecular Hydrogels for Drug Delivery and Stem Cell Encapsulation. Langmuir. 2008; 24:10306–10312. [PubMed: 18680318]
9. Pek YS, Wan ACA, Shekaran A, Zhou L, Ying JYA. Thixotropic Nanocomposite Gel for Three-Dimensional Cell Culture. Nat Nanotechnol. 2008; 3:671–675. [PubMed: 18989333]
10. Guvendiren M, Lu HD, Burdick JA. Shear-thinning injectable hydrogels. Soft Matter. 2012; 8:260–272.
11. Salem AK, et al. Porous Polymer and Cell Composites that Self-Assemble in Situ. Adv Mater. 2003; 15:210–213.
12. Ehrbar M, Schoenmakers R, Christen EH, Fussenegger M, Weber W. Drug-Sensing Hydrogels for the Inducible Release of Biopharmaceuticals. Nat Mat. 2008; 7:800–804.
13. Petka WA, Harden JL, McGrath KP, Wirtz D, Tirrell DA. Reversible Hydrogels from Self-Assembling Artifical Proteins. Science. 1998; 281:389–392. [PubMed: 9665877]
14. Shen W, Zhang KC, Kornfield JA, Tirrell DA. Tuning the Erosion Rate of Artificial Protein Hydrogels Through Control of Network Topology. Nat Mater. 2006; 5:153–158. [PubMed: 16444261]
15. Lu HD, Charati MB, Kim IL, Burdick JA. Injectable Shear-Thinning Hydrogels Engineered with a Self-Assembled Dock-and-Lock Mechanism. Biomaterials. 2012; 33:2145–2153. [PubMed: 22177842]
16. Lu HD, Soranno DE, Rodell CB, Kim IL, Burdick JA. Secondary Photocrosslinking of Injectable Shear-Thinning Dock-and-Lock Hydrogels. Adv Heath Mater. 2013; 2:1028–1036.
17. Rodell CB, Kaminski A, Burdick JA. Rational Design of Network Properties in Guest-Host Assembled and Shear-Thinning Hyaluronic Acid Hydrogels. Biomacromolecules. 2013; 14:4125–4134. [PubMed: 24070551]
18. Nakahata M, Takashima Y, Yamaguchi H, Harada A. Redoxresponsive self-healing materials formed from host-guest polymers. Nat Comm. 2011; 2:511.
19. Park KM, et al. In Situ Supramolecular Assembly and Modular Modification of Hyaluronic Acid Hydrogels for 3D Cellular Engineering. ACS Nano. 2012; 6:2960–2968. [PubMed: 22404424]
20. Appel EA, et al. Supramolecular Cross-Linked Networks via Host–Guest Complexation with Cucurbit[8]uril. J Am Chem Soc. 2010; 132:14251–14260. [PubMed: 20845973]

21. Appel EA, Loh XJ, Jones ST, Dreiss CA, Scherman OA. Sustained release of proteins from high water content supramolecular hydrogels. Biomaterials. 2012; 33:4646–4652. [PubMed: 22459194]
22. Appel EA, et al. High-water-content hydrogels from renewable resources through host-guest interactions. J Am Chem Soc. 2012; 134:11767–11773. [PubMed: 22758793]
23. Rowland MJ, Appel EA, Coulston RJ, Scherman OA. Dynamically Crosslinked Materials via Recognition of Amino Acids by Cucurbituril. J Mater Chem B. 2013; 1:2904–2910.
24. Wang Q, et al. High-Water-Content Mouldable Hydrogels by Mixing Clay and a Dendritic Molecular Binder. English Nature. 2010; 463:339–343.
25. Rose S, et al. Nanoparticle Solutions as Adhesives for Gels and Biological Tissues. Nature. 2014; 505:382–385. [PubMed: 24336207]
26. Wu CJ, Gaharwar AK, Schexnailder PJ, Schmidt G. Development of biomedical polymer-silicate nanocomposites: A materials science perspective. Materials. 2010; 3:2986–3005.
27. Schexnailder PJ, Schmidt G. Nanocomposite polymer hydrogels. Colloid Polym Sci. 2009; 287:1–11.
28. Jin Q, Schexnailder PJ, Gaharwar AK, Schmidt G. Silicate cross-linked bio-nanocomposite hydrogels from PEO and Chitosan. Macromol Biosci. 2009; 9:1028–1035. [PubMed: 19593783]
29. Baumann MD, Kang CE, Tator CH, Shoichet MS. Intrathecal delivery of a polymeric nanocomposite hydrogel after spinal cord injury. Biomaterials. 2010; 31:7631–7639. [PubMed: 20656347]
30. Baumann MD, et al. An injectable drug delivery platform for sustained combination therapy. J Control Release. 2009; 138:205–213. [PubMed: 19442692]
31. Chiellini, E.; Sunamoto, J.; Migliaresi, C.; Ottenbrite, RM.; Cohn, D., editors. Biomedical Polymers and Polymer Therapeutics. Kluwer Academic/Plenum Publishers; 2001.
32. Rubinstein, M.; Colby, RH. Polymer Physics. Oxford University Press; 2003.
33. Biedermann F, et al. Postpolymerization Modification of Hydroxyl-Functionalized Polymers with Isocyanates. Macromolecules. 2011; 44:4828–4835.
34. Hussain S, Keary C, Craig DQM. A thermorheological investigation into the gelation and phase separation of hydroxypropyl methyl-cellulose aqueous systems. Polymer. 2002; 43:5623–5628.
35. Gref R, et al. Biodegradable Long-Circulating Polymeric Nanospheres. Science. 1994; 263:1600–1603. [PubMed: 8128245]
36. Kamaly N, Xiao Z, Valencia PM, Radovic-Moreno AF, Farokhzad OC. Targeted polymeric therapeutic nanoparticles: design, development and clinical translation. Chem Soc Rev. 2012; 41:2971–3010. [PubMed: 22388185]
37. Lohmeijer B, et al. Guanidine and Amidine Organocatalysts for Ring-Opening Polymerization of Cyclic Esters. Macromolecules. 2006; 39:8574–8583.
38. Cheng J, et al. Formulation of Functionalized PLGA-PEG Nanoparticles for In Vivo Targeted Drug Delivery. Biomaterials. 2007; 28:869–876. [PubMed: 17055572]
39. Crank, J. The Mathematics of Diffusion. Clarendon Press; Oxford: 1975.
40. Ritger P, Peppas N. A Simple Equation for Description of Solute Release II: Fickian and Anomalous Release from Swellable Devices. J Controlled Release. 1987; 5:37–42.

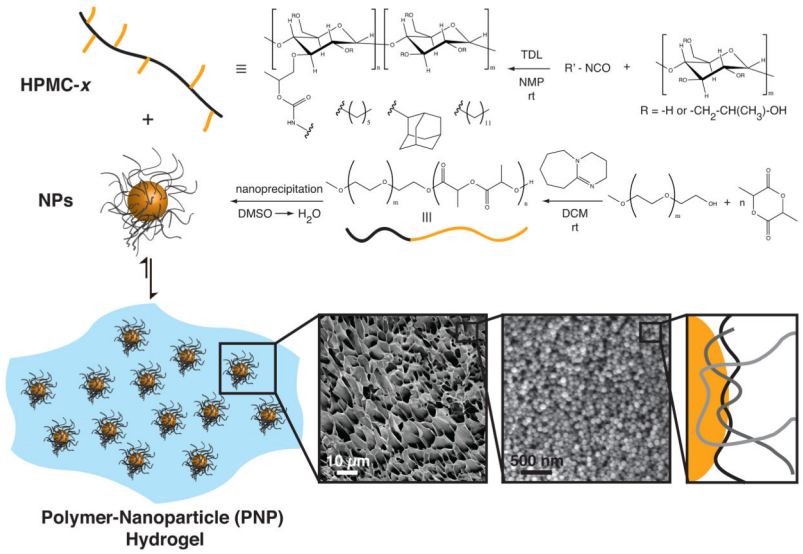

Figure 1. Fabrication of PNP hydrogels from HPMC derivatives and nanoparticles

a. Schematic representation of the preparation of polymer-nanoparticle (PNP) hydrogels utilising non-covalent interactions between core-shell nanoparticles (NPs) and **b.** hydrophobically-modified hydroxypropylmethylcellulose (HPMC-*x*; C_6 - hexyl, Ad - adamantyl, C_{12} - dodecyl). **c.** The NPs can be composed of either poly(styrene) (PS; *non-degradable*) or poly(ethylene glycol)-*block*-poly(lactic acid) (PEG-*b*-PLA; *biodegradable*). **d.** Cryogenic scanning electron microscopy images of PNP gels composed of PSNPs (d ~ 50 nm) demonstrate a homogeneous distribution of NPs within the gel structure, indicating that the network is held together by multivalent, dynamic polymer-nanoparticle interactions (as illustrated; polymer chains - greyscale, nanoparticle - orange).

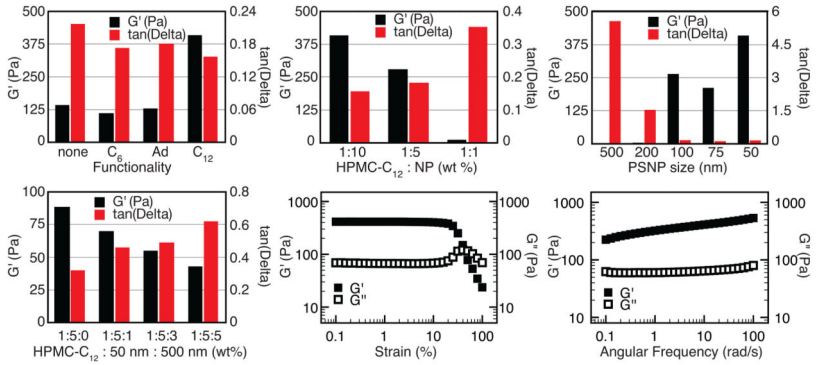

Figure 2. Rheological characterisation of PNP hydrogels from HPMC derivatives and nanoparticles

Oscillatory rheological properties of hydrogels from **a.** HPMC-C_{12} (1 wt%) with PSNPs (10 wt%) of various sizes, **b.** HPMC-C_{12} with PSNP (50 nm) at various loadings, and **c.** HPMC-*x* bearing various functionality (0.5 mmol/g; 1 wt%) with PSNPs (50 nm; 10 wt%). All values collected at $\omega = 10$ rad/s, $\varepsilon = 2\%$, 25°C. **d.** Oscillatory rheological properties of hydrogels from HPMC-C_{12} (1 wt%) with PSNPs of two different sizes: 50 nm (5 wt%) and 500 nm (1, 3 and 5 wt%). The large particles ($D_H \gg l_P$) contribute to a dramatic decrease in the mechanical properties of the PNP gels, even though more particles are being added to the formulation and thus contributing to an increase in the number of polymer-nanoparticle interactions per unit volume (n). **e.** Strain-dependent ($\omega = 10$ rad/s, 25°C) and **f.** frequency-dependent ($\varepsilon = 2\%$, 25°C) oscillatory shear rheology of HPMC-C_{12} (1 wt%)/PSNP (10 wt%) hydrogels.

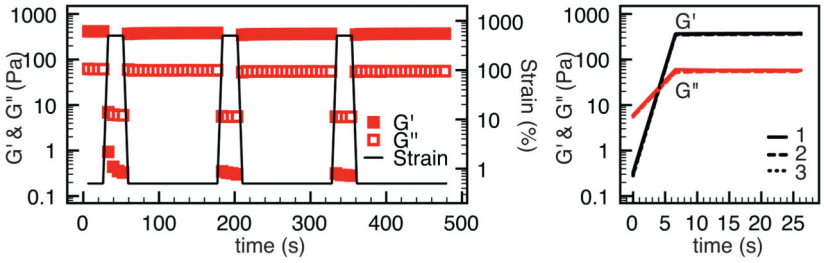

Figure 3. Shear-thinning and self-healing behaviour of PNP hydrogels

a. Step-strain measurements of HPMC-C_{12} (1 wt%)/PSNP (10 wt%) hydrogels over three cycles (ω = 10 rad/s, 25°C) with **b.** overlayed zoom of the recovery of material properties after each cycle.

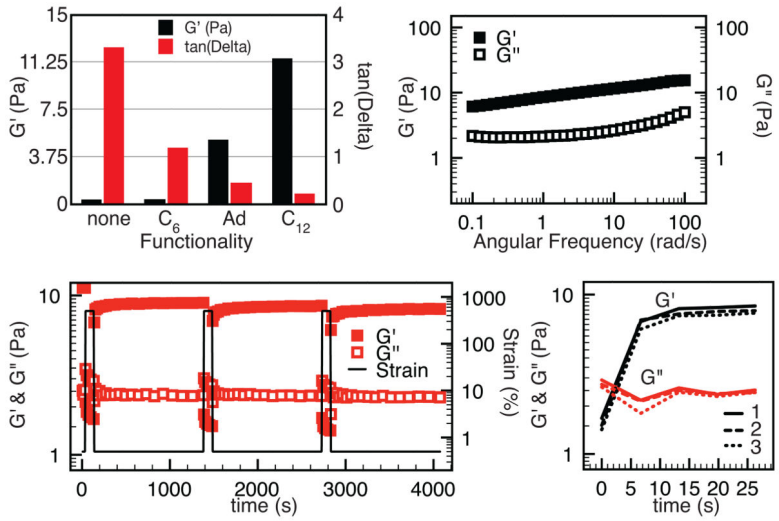

Figure 4. Rheological characterisation of biodegradable PNP hydrogels

a. Oscillatory rheological properties of hydrogels from HPMC-*x* bearing various functionality (0.5 mmol/g; 1 wt%) with PEG-*b*-PLA NPs (10 wt%; $\omega = 10$ rad/s, $\varepsilon = 2\%$, 37°C). **b.** Frequency-dependent ($\varepsilon = 2\%$, 37°C) oscillatory shear rheology of HPMC-C_{12} (1 wt%)/PEG-*b*-PLA NPs (10 wt%) hydrogels. **c.** Step-strain measurements of HPMC-C_{12} (1 wt%)/PEG-*b*-PLA NPs (10 wt%) hydrogels over three cycles ($\omega = 10$ rad/s, 37°C) with **d.** overlayed zoom of the recovery material properties after each cycle.

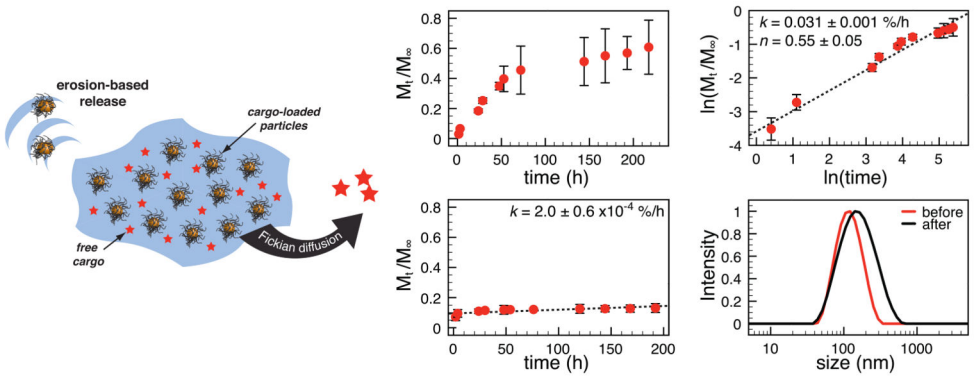

Figure 5. *In vitro* controlled delivery by differential mechanisms simultaneously

a. Schematic representation of two stage release of therapeutic cargo. **b.** Drug release profiles Bovine Serum Albumin (BSA; *hydrophilic*) from hydrogels showing the cumulative proportion of "drug" released (M_t/M_∞; the cumulative fractional mass released at time *t*; n = 3; data presented as mean ± s.e.m.). **c.** Fitting of the release data clearly indicates that the BSA is releasing from the hydrogel by Fickian diffusion with a diffusional release coefficient, *k*, of 0.031± 0.001 %/h. **d.** Drug release profile of Oil Red (OR; *hydrophobic*) from hydrogels prepared with OR-loaded PEG-*b*-PLA NPs (n = 3; data presented as mean ± s.e.m.). In this case, OR is released exclusively by erosion from the hydrogel surface (*k* = 2.0± 0.6 ×10^{-4} %/h) following a small burst release (< 10%). **e.** Dynamic light scattering (DLS) characterisation of PEG-*b*-PLA NPs (as prepared before hydrogel formation) and the supernatant following erosion of PNP hydrogels (*i.e.* after release of NPs) supporting the proposed erosion-based release mechanism.

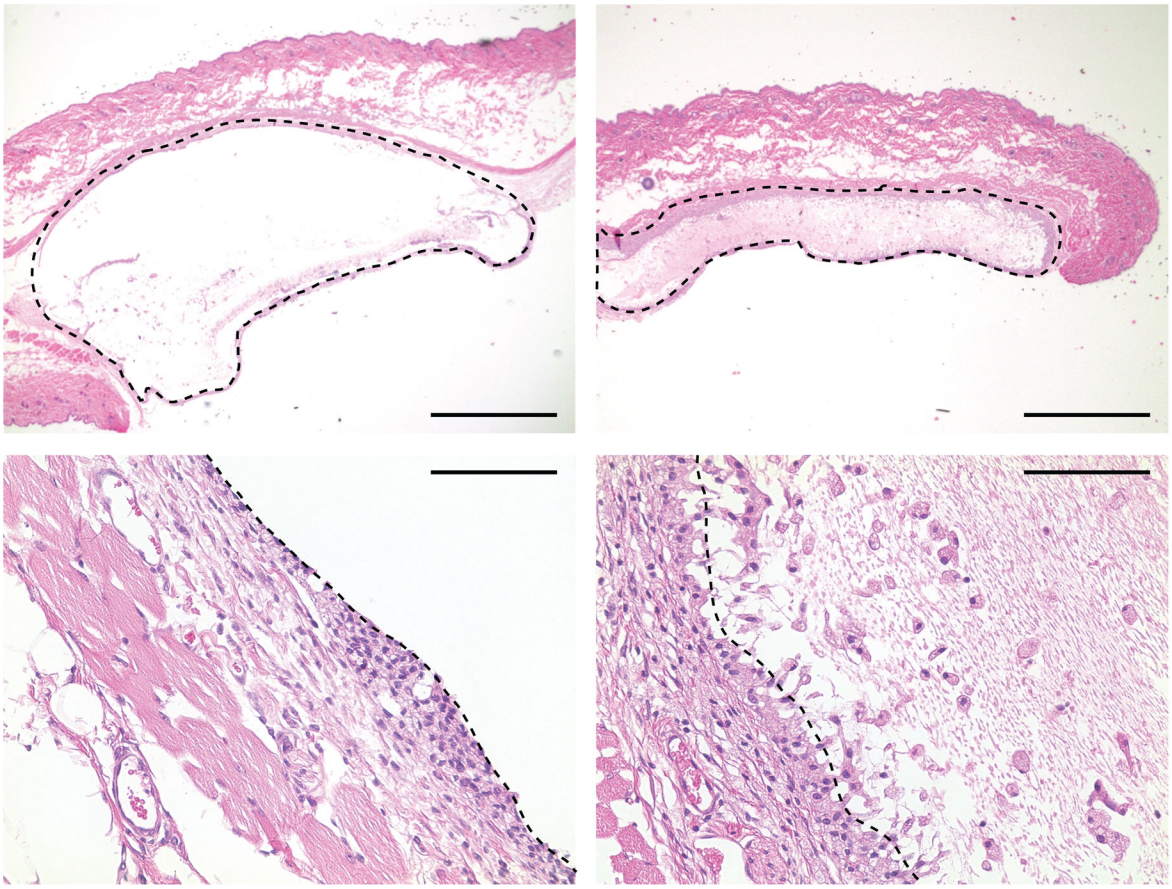

Figure 6. ***In vivo*** **biocompatibility**

Histological anaylsis of haematoxylin stained samples taken after 3 days (**a.** 2× and **c.** 40×) and 7 days (**b.** 2× and **d.** 40×) *in vivo*. In each image, the interface between biological tissue and PNP gel is denoted with a dotted line. Scale bar = 2000 μm (2×) and 100 μm (40×).

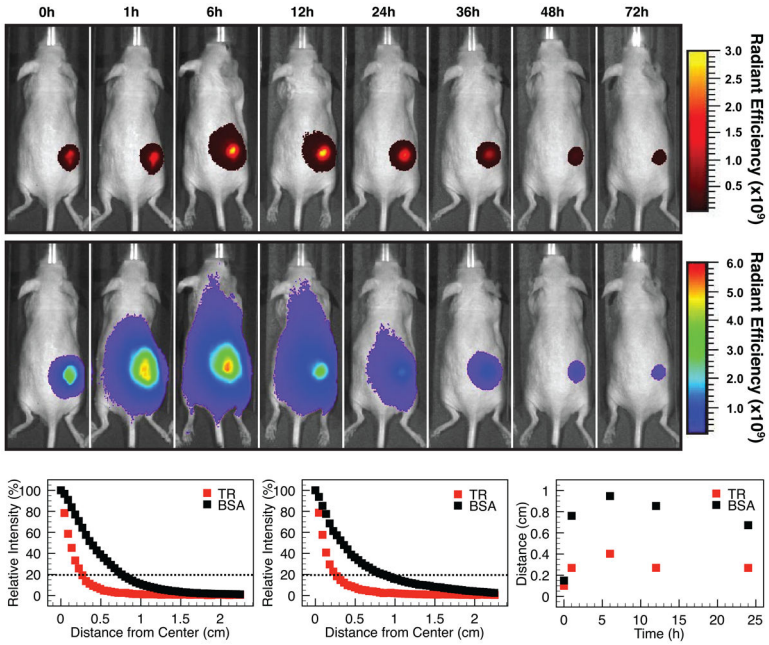

Figure 7. ***In vivo*** **dual-therapeutic release**

a. Intravital fluorescence imaging of the release of TR (top) and BSA-AF (bottom) from a single material. Plots of relative intensity of model therapeutic fluorescence *vs.* distance from the center of the hydrogel implant (n = 5) at **b.** 1h and **c.** 12h. **d.** Radius of release at 20% relative fluorescence intensity over time (n = 5).